ELSEVIER

Nuclear Physics A 612 (1997) 213–222

NUCLEAR PHYSICS A

Measurement of double-differential (n, xp) cross sections of natural nickel in 14.6 MeV neutron energy

Bangjiao Ye, Zhongmin Wang, Yangmei Fan, Rongdian Han

University of Science and Technology of China, Department of Modern Physics, Hefei Anhui 230026, People's Republic of China

Zhenxi Xiao

University of Science and Technology of China, Institute of Management, Beijing 100080, People's Republic of China

Received 12 June 1995; revised 30 September 1996

Abstract

The energy spectra and angular distributions of proton emission in the reaction of ^{nat}Ni(n, xp) at neutron energy 14.6 MeV have been measured by the USTC multitelescope system. The double-differential cross sections of 16 reaction angles from 25° to 164.5° have been obtained in this measurement. The statistical error can be reduced because of the thick target used. The angular distributions show a slightly energy-dependent forward–backward asymmetry. The angle-integrated proton spectrum is compared with ENDF/B-VI evaluation and Grimes' result. The total p-emission cross section is in fair agreement with prediction and evaluation.

Keywords: NUCLEAR REACTION ^{nat}Ni(n, xp); $E = 14.6$ MeV; Measured $\sigma(\theta_p, E_p)$; Angle-integrated σ, total p-emission σ.

1. Introduction

The reactions of neutrons with structural materials to produce emitted charged particles are important in the design of fission and fusion reactors. The (n, xp) and (n, $x\alpha$) reactions lead to nuclear transmutation, which can affect the structural strength of the materials. They also produce recoils from the lattice, leading to voids and missing lattice elements. Finally, they lead to buildup of hydrogen and helium gas and residual

PII S0375-9474(96)00394-6

radioactivity. Knowing the strength, radioactivity and lifetime of structural materials is of great economic importance.

Two techniques are generally used to measure neutron-induced charged- particle emitted reaction cross sections: direct detection of charged particles emitted (with time-of-flight spectrometer, magnetic quadrupole spectrometers and multitelescope system) and detection of radiation emitted by the radioactive residual nuclei. These methods have their own advantages and limitations. The radiochemical measurements are feasible only in certain cases where residual nuclei reached by the charged-particle emission are unstable. Also, such measurements do not provide the energy spectrum and angular distribution information that is useful in estimating nuclear recoil energies in the lattice. At neutron energies near 15 MeV, several reaction channels are likely to be open. For example, the (n,xp) cross section is the sum of (n,p), (n,n′p), (n,pn′), and possibly the (n,2p) channels. The radiochemical method does not allow a distinction between (n,d) and (n,n′p) or (n,pn′) processes, as all of these lead to the same final nucleus. Direct detection of charged particles is more difficult experimentally because of low counting rates and high backgrounds. With this method, angular and energy distributions can be obtained.

Over the past 20 years, some new detection systems have been developed to detect the charged particles emitted, for example, the charged-particle time-of-flight (TOF) spectrometer at Ohio University [1], the magnetic quadrupole spectrometer at LLNL [2] and the multitelescope system at Vienna University [3] and University of Science and Technology of China (USTC) [4]. The energy and angular distribution of the emission of protons, deuterons, and alpha particles in the neutron energy range < 15 MeV with some structural materials have been studied [5–8]. Nickel is a very important structural material in nuclear engineering, so its data is very useful for the evaluation of radiation-induced material damage, radiation safety, neutron dosimetry, etc. Based on this aim, the double-differential proton emission cross sections have been measured in USTC using the multitelescope system. Thick targets were used in this measurement and the double-differential cross sections (DDCS) were derived by unfolding the thick-target spectra. In this way it is possible to measure the high-energy parts of the spectra with much better accuracy at the same time than with the thin-target method and also the results are much less sensitive to the background.

2. Experimental procedure

Neutrons of 14.6 MeV were produced by the 150-KV Cockcroft–Walton accelerator at USTC. The multitelescope system is similar to the Vienna system [3], which was described in great detail in Ref. [4]. The schematic diagram of the USTC system is shown in Fig. 1. Here only some brief introduction to this experiment is given.

A natural nickel target with a pureness 99.9%, thick compared to the range of the most energetic (about 15 MeV) protons was desired. A metallic Ni sheet 0.5 mm thick and 40 mm long was used. The whole chamber consist of 32 telescopes. 16 telescopes

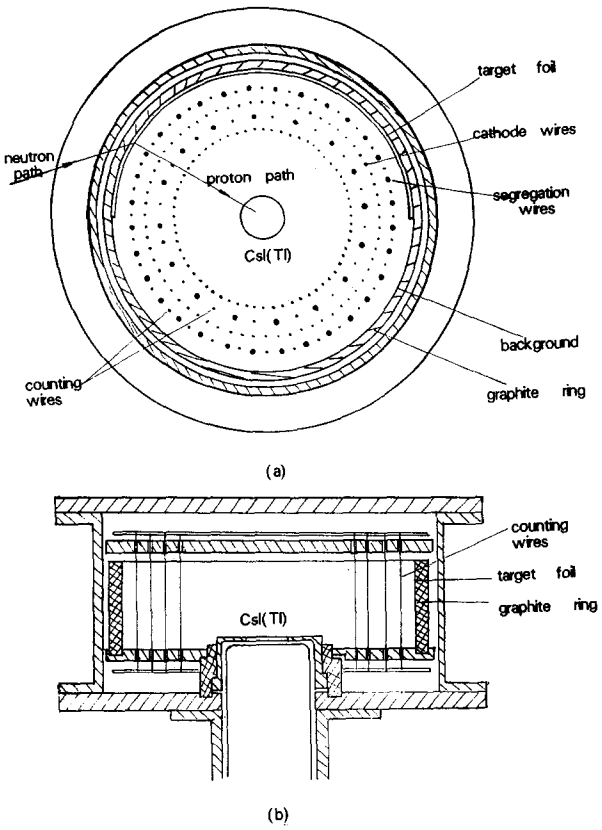

Fig. 1. The USTC multitelescope system: (a) top view and (b) side view.

were used for the measurement of nickel targets which were fixed in the ring-shape graphite holder and the other 16 telescopes were used for simultaneous measurement of the background. Graphite was used for the target holder and background-measuring material because it has a very large negative Q-value (-12.7 MeV) and very small cross sections of the (n,p) reaction. The proportional counters were operated with a gas mixture of 5% CO_2 + 95% Ar at a gas pressure of 100 mb at a voltage of -750 V.

A CsI(Tl) crystal with 1 mm height and 25.4 mm diameter was used as the energy detector. 20 cm Fe was used as shielding material to shield CsI(Tl) from neutrons. The distance between the neutron source (T–Ti target) and CsI(Tl) is 400 mm. Monte Carlo methods (10^6 events) were used for calculation of the reaction angular distribution function according to their geometric relation [9].

The whole system was irradiated for about 50 h at a neutron source strength $\sim 1.5 \times 10^9$ n/s. During the entire experiment, one background telescope was equipped with a weak ^{241}Am α -source, and another was equipped with polyethylene foil. These telescopes were used to monitor the energy calibration of the CsI(Tl) crystal. The stability of the entire measuring system was checked continually by monitoring all the

important single counter rates. The target foil was rotated 180° at the midpoint of the experiment to reduce the asymmetry effects due to the two different halves of the reaction chamber. The total number of true events turned out to be ~ 450 000.

3. Data analysis and results

The whole experiment was controlled by an intelligent CAMAC crate controller. Data collected were recorded in the buffer region of the CAMAC crate controller. When the buffer region was full or the collection of data was complete, the data were read out and stored on disk by the host computer.

For each Ni(n, xp) reaction five-parameter data were recorded on computer disk in this experiment. These are the energy loss signal (ΔE), the wire address signal (θ) from which the reaction angle can be derived, the time-of-flight signal (TOF) of charged particle, the energy signal (E) and the pulse shape discrimination signal (PSD) in the CsI(Tl) crystal.

Data analysis was performed in several steps: First, by selecting the appropriate channel range in the TOF spectra, the PSD spectra and $E \cdot \Delta E$ spectra, the chance coincidence counts, alpha particles and gamma rays were eliminated. Second, the true background was eliminated by subtraction of the background energy spectra from the corresponding foreground energy spectra, channel by channel. In this way, thick-target

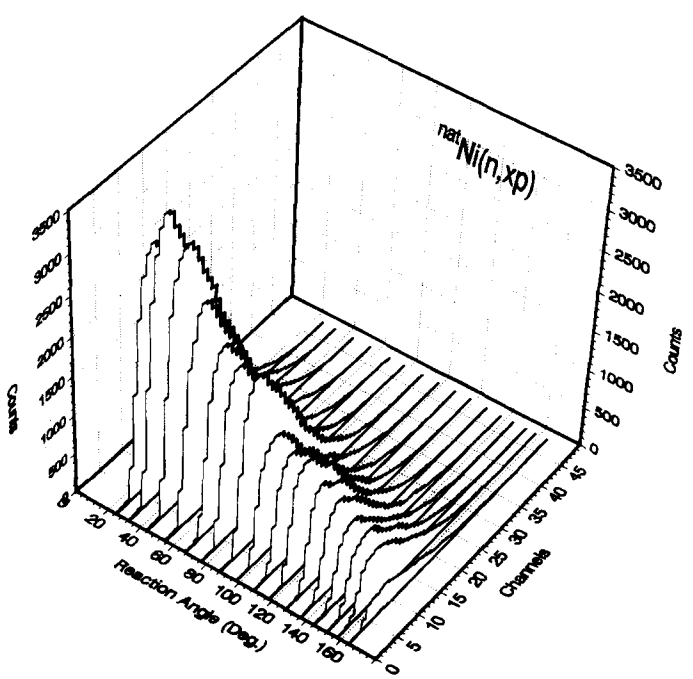

Fig. 2. Thick-target proton energy spectra were obtained from this experiment for 16 reaction angles.

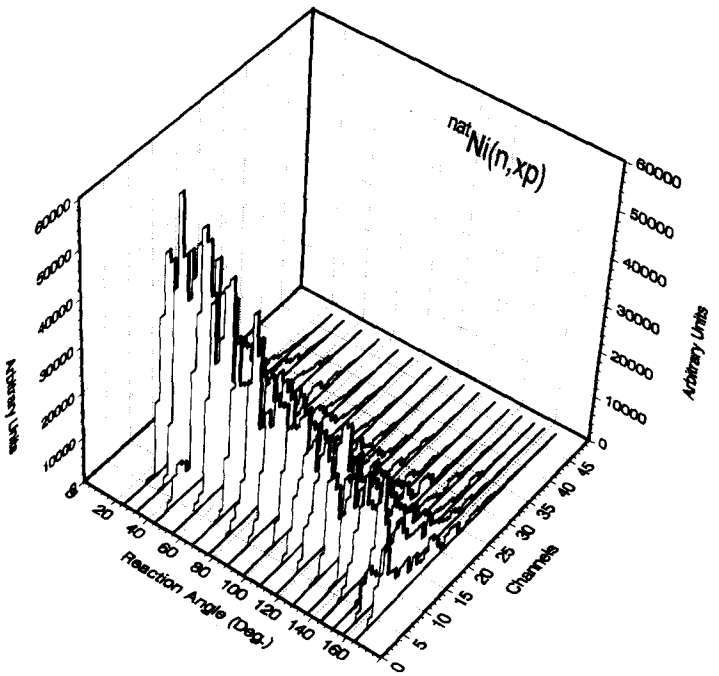

Fig. 3. Equivalent thin-target spectra were obtained by unfolding the thick targets spectra of Fig. 1.

proton energy spectra were obtained for 16 reaction angles from 25.0° to 164.5° and shown in Fig. 2. Third, to obtain the proton emission spectra the measured "thick target" spectra $N(E_p)$ had to be unfolded. This was done by numerically differentiating the quantity $(dE_p/dX) \cdot N(E_p)$ with respect to E_p. This process was similar to that of Ref. [8]. After this step, all thick-target spectra were transformed into equivalent thin-target spectra, shown in Fig. 3. These results are all in the laboratory system. Conversion of these results to the c.m. system has been done, however, the angle-integrated energy spectra in the c.m. system as well as the laboratory system should be similar, since the target nuclei have large masses.

The double-differential proton emission cross sections were obtained at 16 reaction angles with an angular resolution of 12° on average. Both experimental data and their errors are listed in Table 1 in the c.m. system. The errors in Table 1 consist of statistical errors and all identified systematic error contributions. The statistical error corresponding to 1σ error was small because of the large number of true events in this measurement. The total systematic error is 6.2% which consists of the neutron flux error 3.3%, the target height error 2%, the solid angle of the central detector error 3%, the dE/dx value error 2%, the data reduction procedure error 2%, and other uncertainties possibly 3%.

Because of high background counts at low energy, the DDCS of proton emission were not extracted below 3 MeV. The proton energy for 3 to 4 MeV could only be measured at six angles, which are also listed in Table 1.

Table 1
DDCS of the ^{nat}Ni(n, xp) reaction at $E_n = 14.6$ MeV in the c.m. system

E_p (MeV)	Reaction angles (Deg)							
	25.6	33.6	44.9	56.1	68.5	78.4	89.7	99.7
3–4	11.66 ± 0.74	11.28 ± 0.71			10.00 ± 0.63	12.31 ± 0.77		
4–5	10.55 ± 0.67	12.04 ± 0.88	12.21 ± 0.77	11.08 ± 0.70	11.34 ± 0.71	11.89 ± 0.75	12.12 ± 0.76	13.16 ± 0.83
5–6	7.53 ± 0.48	9.62 ± 0.49	11.90 ± 0.75	9.88 ± 0.62	9.77 ± 0.61	9.11 ± 0.58	9.53 ± 0.60	9.56 ± 0.61
6–7	9.02 ± 0.57	8.84 ± 0.56	7.42 ± 0.47	6.55 ± 0.42	6.04 ± 0.38	7.97 ± 0.50	6.64 ± 0.42	8.48 ± 0.54
7–8	6.88 ± 0.43	6.93 ± 0.44	5.51 ± 0.35	5.42 ± 0.34	5.26 ± 0.33	4.89 ± 0.31	5.45 ± 0.35	4.26 ± 0.29
8–9	3.62 ± 0.23	2.54 ± 0.17	3.02 ± 0.20	3.20 ± 0.21	3.62 ± 0.23	2.58 ± 0.17	2.45 ± 0.16	3.23 ± 0.21
9–10	1.77 ± 0.12	1.89 ± 0.12	2.36 ± 0.15	1.63 ± 0.11	1.38 ± 0.10	1.99 ± 0.13	1.68 ± 0.11	1.63 ± 0.12
10–11	1.04 ± 0.7	1.31 ± 0.09	0.88 ± 0.06	0.86 ± 0.06	0.86 ± 0.06	0.98 ± 0.07	0.73 ± 0.05	1.17 ± 0.09
11–12	0.54 ± 0.04	0.60 ± 0.04	0.70 ± 0.05	0.47 ± 0.4	0.48 ± 0.04	0.56 ± 0.04	0.38 ± 0.03	0.78 ± 0.06
12–13	0.30 ± 0.02	0.31 ± 0.02	0.36 ± 0.03	0.32 ± 0.02	0.21 ± 0.02	0.23 ± 0.02	0.23 ± 0.02	
13–14	0.16 ± 0.01	0.11 ± 0.01	0.11 ± 0.01	0.11 ± 0.01	0.09 ± 0.01	0.04–0.01	0.10 ± 0.01	0.14 ± 0.01

E_p (MeV)	Reaction angles (Deg)							
	109.9	119.1	129.1	137.5	145.1	152.5	158.3	164.9
3–4		11.74 ± 0.62	11.27 ± 0.71					
4–5	9.65 ± 0.62	12.75 ± 0.93	8.99 ± 0.51	7.68 ± 0.49	10.51 ± 0.67	9.10 ± 0.76	7.56 ± 0.49	3.90 ± 0.27
5–6	9.93 ± 0.63	11.50 ± 0.72	9.53 ± 0.66	9.00 ± 0.57	8.95 ± 0.57	8.54 ± 0.36	7.43 ± 0.47	3.23 ± 0.23
6–7	6.86 ± 0.44	5.96 ± 0.38	7.17 ± 0.46	7.77 ± 0.49	5.41 ± 0.35	5.76 ± 0.37	3.07 ± 0.21	3.09 ± 0.21
7–8	4.74 ± 0.30	5.23 ± 0.34	3.27 ± 0.22	3.98 ± 0.26	3.82 ± 0.25	4.46 ± 0.29	4.08 ± 0.27	0.81 ± 0.09
8–9	2.33 ± 0.16	3.03 ± 0.20	2.89 ± 0.19	2.44 ± 0.16	2.11 ± 0.14	1.79 ± 0.13	1.50 ± 0.11	1.16 ± 0.10
9–10	2.42 ± 0.16	1.46 ± 0.10	1.62 ± 0.11	1.08 ± 0.09	1.39 ± 0.10	1.06 ± 0.08	1.14 ± 0.08	1.04 ± 0.09
10–11	0.59 ± 0.05	1.09 ± 0.08	0.72 ± 0.06	0.66 ± 0.06	0.63 ± 0.05	0.66 ± 0.05	1.15 ± 0.08	0.07 ± 0.04
11–12	0.63 ± 0.5	0.53 ± 0.04	0.60 ± 0.04	0.67 ± 0.05	0.39 ± 0.03	0.48 ± 0.04	0.25 ± 0.03	0.19 ± 0.03
12–13	0.16 ± 0.02	0.15 ± 0.02	0.19 ± 0.02	0.24 ± 0.02	0.13 ± 0.02	0.05 ± 0.01	0.13 ± 0.02	0.05 ± 0.02
13–14	0.16 ± 0.02	0.05 ± 0.01	0.14 ± 0.01	0.09 ± 0.01	0.07 ± 0.01	0.04 ± 0.01	0.01 ± 0.01	0.13 ± 0.01

Table 2
Angle-integrated cross sections of the ^{nat}Ni(n, xp) reaction at $E_n = 14.6$ MeV

E_p (MeV)	$d\sigma/dE_p$ (mb)
3–4	142.7 ± 9.0
4–5	133.9 ± 11.5
5–6	117.4 ± 13.8
6–7	84.1 ± 8.7
7–8	60.1 ± 8.5
8–9	33.7 ± 2.8
9–10	20.2 ± 1.7
10–11	10.3 ± 1.6
11–12	6.4 ± 0.8
12–13	2.9 ± 0.3
13–14	1.1 ± 0.3

The angle-integrated proton emission cross sections were derived from least-squares fits of Legendre polynomials up to $l = 2$ to the $(d^2\sigma/dE_p\, d\theta)$ values. The results of this calculation are listed in Table 2. The total proton emission cross section for proton energy > 3 MeV is 612.8 ± 44.8 mb.

4. Comparison with other results and discussion

The angular distributions of proton emission from this measurement are shown in Fig. 4 in 2 MeV bins. The solid lines in this figure are the predictions of systematics of

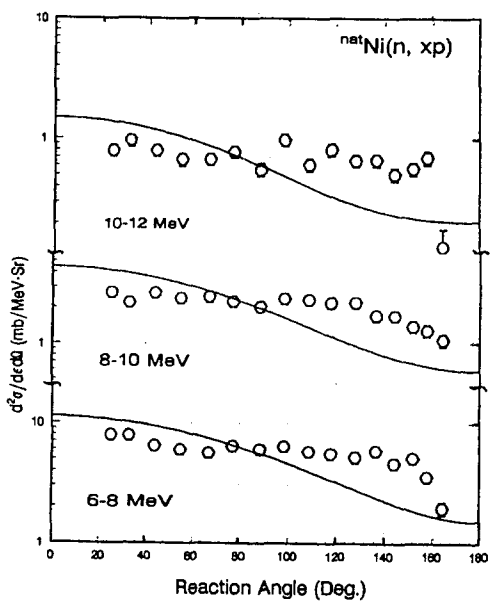

Fig. 4. The angular distributions of p-emission from ^{nat}Ni(n, xp) reaction in 2 MeV energy regions. The solid lines are the predictions of the systematics of Kalbach and Mann.

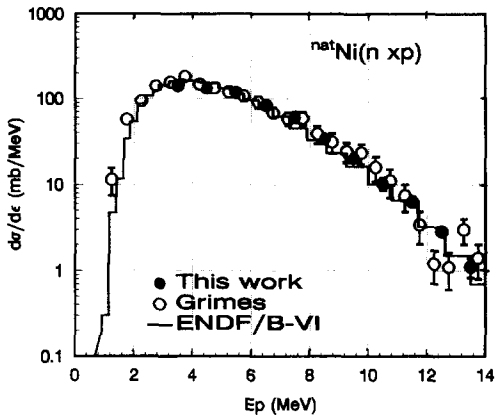

Fig. 5. Proton spectra from the ^{nat}Ni(n, xp) reaction and the evaluation result of ENDF/B-VI library.

Kalbach and Mann [10], where the values of $a_0^{MSD}(\varepsilon_p)/(a_0^{MSD}(\varepsilon_p) + a_0^{MSC}(\varepsilon_p))$ are 0.4, 0.6 and 0.8 for $\varepsilon_p = 6$–8, 8–10 and 10–12 MeV, where the differential cross sections $a_0^{MSD}(\varepsilon_p)$ and $a_0^{MSC}(\varepsilon_p)$ are for MSD and MSC processes. It shows that the angular distribution of proton emission from the natural nickel (n, xp) reaction is not so strong as the Kalbach–Mann predictions [11]. A similar behaviour has been found in the proton spectrum from the natural iron (n, xp) reaction. A possible explanation is that angular distribution may be perturbed by the magnetic hyperfine interaction when the target is ferromagnetic [12].

In 1979, Grimes et al. [12] obtained their measurement results for ^{58}Ni, ^{60}Ni and natural nickel (n, xp) reactions at $E_n = 14.8$ MeV. Their data have been extensively used to test the nuclear reaction models. Comparison of the present result of angle-integrated cross sections with Grimes' result is given in Fig. 5. These data are in fair agreement with Grimes' data, but appear to have better statistics. Further, this result has been compared with the evaluated data of the ENDF/B-VI [15] library which is also given in Fig. 5. It shows that the evaluation of ENDF/B-VI for natural nickel is in good agreement with this result.

The evaluations of total (angle–energy-integrated) p-emission cross sections have

Table 3
Proton-emission cross section of the Ni(n, xp) reaction (mb)

Isotopes and their abundance in the natural nickel		Evaluation				Measurement S.M. Grimes ($E_n = 14.8$ MeV)
		CNDC	BROND	B-VI ($E_n = 14.1$ MeV)	JENDL-3	
68.077%	^{58}Ni	946	898	953	923	1002 ± 120
26.223%	^{60}Ni	270	209	279	137	325 ± 40
1.140%	^{61}Ni	106		185		
3.634%	^{62}Ni	34	22	32.5	28.4	
0.926%	^{64}Ni	5.3		3.2		

Table 4
Proton-emission cross section of the natural nickel (n,T_{xp}) reaction (mb)

Proton energy (MeV)	Evaluation				Grimes (E_n = 14.8 MeV)	USTC (E_n = 14.6 MeV)
	CNDC	BROND (E_n = 14.1 MeV)	B-VI	JENDL-3		
1–14	717.3	668 [a]	725	695	790 ± 100	
3–14			626		643 ± 85	613 ± 45

[a] Because we have not evaluation data for ^{61}Ni and ^{64}Ni, CNDC' data were used.

been carried out by CNDC [13], BROND [14], ENDF/B-VI [15] and JENDL-3 [16] for Ni. These results and Grimes's data are shown in Table 3. Comparisons of Grimes's data with those measured by the activation method demonstrate that almost all Grimes's measurements on p-emission cross sections are higher by about 10 to 15% systematically than others [13]. The evaluations of p-emission from natural nickel in Table 4 are obtained from Table 3 by adding results for all isotopes according to their abundance. Experimental results of Grimes [17] and present work are also listed in Table 4 for $E_p > 3$ MeV, the present result for natural nickel is lower by 5% than Grimes' data.

Acknowledgments

The authors would like to thank CNDC for their support, and thanks to Profs. D.L. Zhou, Q.B. Shen and T.J. Liu for their kind help and suggestions. This work was supported in part by the General Company of Nuclear Industry of China and the Young Funds of USTC.

References

[1] S. Saraf, C. Brient, P. Egun, S. Grimes, V. Mishra and R. Pedroni, Nucl. Sci. Eng. 107 (1991) 365.
[2] S. Grimes, R. Haight, K. Alvar, H. Barschall and R. Borchers, Phys. Rev. C 19 (1979) 2127;
see also S. Grimes and R. Haight, Phys. Rev. C 17 (1978) 508.
[3] G. Traxler, R. Fischer and H. Vonach, Nucl. Instr. Meth. 217 (1983) 121.
[4] B.J. Ye, Y.M. Fan, Z.M. Wang, R.D. Han, W. Mei, X.Q. Yu, Y.M. Yang, R.Y. Han, H.J. Du and Z.X. Xiao, Commun. Nucl. Data Progr. 10 (1993) 19.
[5] S. Graham, M. Ahmad, S. Grimes, H. Satyanarayana and S. Saraf, Nucl. Sci. Eng. 95 (1987) 60.
[6] M. Ahmad, S. Graham, S. Grimes, H. Satyanarayana, S. Saraf and S. Stricklin, Nucl. Sci. Eng. 90 (1985) 311.
[7] G. Traxler, A. Chalupka, R. Fischer, B. Strohmaier, M. Uhl and H. Vonach, Nucl. Sci. Eng. 90 (1985) 174;
see also, R. Fischer, M. Uhl, and H. Vonach, Phys. Rev. C 37 (1988) 68.
[8] B.J. Ye, Y.M. Fan, Z.M. Wang, R.D. Han and Z.X. Xiao, Nucl. Sci. Eng. 117 (1994) 67.
[9] G. Lin and B.J. Ye, J. China Univ. Sci. Tech. 25 (1995) 94.
[10] C. Kalbach and F.M. Mann, Phys. Rev. C 23 (1981) 112;
see also C. Kalbach, Phys. Rev. C 25 (1982) 3197.
[11] B.J. Ye, Y.M. Fan, Z.M. Wang, R.D. Han and Z.X. Xiao, Nucl. Sci. Eng. (to be published).
[12] T.U. Chan, M. Agard, J. Bruandet, A. Giorni, F. Glaser, J. Longequeue and C. Morand, J. Phys. Lett. (Paris) 10 (1976) 237.

[13] Chinese Nuclear Data Center (CNDC), D. Zhou, J. Zhang and T. Liu, Final Report for IAEA Contract Nr. 5962/R1/RB.
[14] USSR Evaluated Neutron Data Library (BROND-2), Y.N. Manokhin et al., IAEA-NDS-90 (Rev. 3) 1990.
[15] Evaluated Nuclear Data File (ENDF/B-VI) Summary Documentation, Report BNL-NCS-17541, Oct. 1991.
[16] Japanese Evaluated Nuclear Data Library (JENDL-3), Y. Kikuchi, IAEA-NDS-110, 1990.
[17] Grimes' data of natural nickel were provided by Q.C. Lian, Nucl. Data Library, Chinese Nuclear Data Center (CNDC).